



# An effective kinase inhibition strategy for metastatic recurrent childhood medulloblastoma

Ashley A. Adile<sup>1,2</sup> · David Bakhshinyan<sup>1,2</sup> · Yujin Suk<sup>1,2</sup> · David Uehling<sup>6</sup> · Mehakpreet Saini<sup>6</sup> · Ahmed Aman<sup>6,7</sup> · Jakob Magolan<sup>2</sup> · Minomi K. Subapanditha<sup>1,2</sup> · Dillon McKenna<sup>1,2</sup> · Chirayu Chokshi<sup>1,2</sup> · Neil Savage<sup>1,2</sup> · Michelle M. Kameda-Smith<sup>1,2,3</sup> · Chitra Venugopal<sup>1,3</sup> · Sheila K. Singh<sup>1,2,3,4,5</sup>

Received: 6 May 2023 / Accepted: 13 June 2023 / Published online: 24 June 2023  
© The Author(s), under exclusive licence to Springer Science+Business Media, LLC, part of Springer Nature 2023

## Abstract

**Purpose** Medulloblastomas (MBs) constitute the most common malignant brain tumor in children and adolescents. *MYC*-amplified Group 3 MBs are characterized by disease recurrence, specifically in the leptomeninges, whereby patients with these metastatic tumors have a mortality rate nearing 100%. Despite limited research on such tumors, studies on MB metastases at diagnosis suggest targeting kinases to be beneficial.

**Methods** To identify kinase inhibitors that eradicate cells driving therapy evasion and tumor dissemination, we utilized our established patient-derived xenograft (PDX) mouse-adapted therapy platform that models human MB metastatic recurrences following standard chemoradiotherapy. High-throughput screens of 640 kinase inhibitors were conducted against cells isolated from mouse spines in the PDX model and human fetal neural stem cells to reveal compounds that targeted these treatment-refractory, metastatic cells, whilst sparing healthy cells. Blood–brain barrier permeability assays and additional in vitro experimentation helped select top candidates for in vivo studies.

**Results** Recurrent Group 3 MB PDX spine cells were therapeutically vulnerable to a selective checkpoint kinase 1 (CHK1) inhibitor and small molecular inhibitor of platelet-derived growth factor receptor beta (PDGFR $\beta$ ). Inhibitor-treated cells showed a significant reduction in MB stem cell properties associated with treatment failure. Mice also demonstrated survival advantage when treated with a CHK1 inhibitor ex vivo.

**Conclusion** We identified CHK1 and PDGFR $\beta$  inhibitors that effectively target MB cells fueling treatment-refractory metastases. With limited research on effective therapies for Group 3 MB metastatic recurrences, this work highlights promising therapeutic options to treat these aggressive tumors. Additional studies are warranted to investigate these inhibitors' mechanisms and recommended in vivo administration.

**Keywords** Recurrent medulloblastoma · Spinal metastases · High-throughput screening · Kinase inhibitors

✉ Sheila K. Singh  
ssingh@mcmaster.ca

<sup>1</sup> Centre for Discovery in Cancer Research, McMaster University, 1280 Main Street West, Hamilton, ON L8S 4L8, Canada

<sup>2</sup> Department of Biochemistry and Biomedical Sciences, McMaster University, 1280 Main Street West, Hamilton, ON L8S 4L8, Canada

<sup>3</sup> Department of Surgery, Faculty of Health Sciences, McMaster University, 1280 Main Street West, Hamilton, ON L8S 4K1, Canada

<sup>4</sup> Human Cancer Stem Cell Biology, McMaster University, 1280 Main Street West, Hamilton, ON L8S 4K1, Canada

<sup>5</sup> Neurosurgery, McMaster Children's Hospital, McMaster University, 1280 Main Street West, Hamilton, ON L8S 4K1, Canada

<sup>6</sup> Ontario Institute for Cancer Research, MaRS Centre, Toronto, ON M5G 0A3, Canada

<sup>7</sup> Leslie Dan Faculty of Pharmacy, University of Toronto, Toronto, ON, Canada

## Introduction

Accounting for nearly 20% of all childhood central nervous system (CNS) neoplasms, medulloblastoma (MB)—an embryonal tumor that originates in the cerebellum, is the most common malignant pediatric brain tumor [1]. Advancements in diagnostic testing, imaging techniques, as well as molecular and histopathological analyses have aided in standardizing multimodal treatment protocols. This consists of maximal safe surgical resection, adjuvant craniospinal irradiation and cytotoxic chemotherapy regimens, which significantly increased the 5-year overall survival to as high as 85% for standard-risk pediatric patients with no residual disease or metastasis [2–4]. However, survivorship of high-risk patients can range from 30 to 70% depending on age; universal to these patients is disease progression at either local (brain) and/or metastatic (spinal leptomeninges) sites.

Our knowledge of MB is largely based on examining bulk tumors from diagnosis combined with clinical parameters that led to the stratification of four distinct molecular subgroups (WNT, SHH, Group 3 & Group 4) [5–7]. Group 3 MBs are often associated with tumor progression and have a greater propensity to metastasize in comparison to other MB subgroups (40–45%) and other CNS tumors [8, 9]. Integrative genomic profiling of primary MB samples underscores the intra-subgroup heterogeneity and correlation to clinical outcome, and demonstrating that Group 3 $\gamma$  MB constitutes the worst prognosis amongst all subtypes (41.9% 5-year survival) [10]. Most often present in infants and young children, Group 3 $\gamma$  MB involves *v-myc* avian myelocytomatosis viral oncogene homolog (*MYC*) amplification and a high frequency of disease metastasis.

Consequently, therapeutic regimens deemed effective for these treatment-naïve specimens are often poised to fail in treatment-refractory lesions due to the complexity of both recurrent and metastatic MB. Current research in commercially-available MB cell lines has highlighted various signaling pathways and targets integral to MB progression and metastasis—most notably phosphatidylinositol 3-kinase (PI3K)/AKT- and Ras/MAPK- pathways, as well as platelet-derived growth factor receptors (PDGFRs) [11–17]. However, mortality rates of relapsed Group 3 $\gamma$  MB patients with leptomeningeal disease dissemination remains fatal in nearly all cases [2, 18]. Development of novel therapies is encumbered by the rare clinical opportunities for these often-inoperable specimens to be collected, and the paucity of mouse models able to recapitulate metastatic MB recurrence.

We previously reported our established patient-derived xenograft (PDX) mouse-adapted therapy model, which provides a reliable platform to recapitulate treatment

administered to MB patients [19]. It enables harvesting of the rare treatment-refractory sub-population of MB cells, termed brain-tumor-initiating cells (BTICs), which retain somatic stem cell properties to drive MB progression, evasion of conventional therapies, and metastasis [20–22]. Prior research have commonly used commercially-available cell lines from MB diagnosis, which merely provides information on the primary disease. However, our goal was to study the metastatic recurrences of *MYC*-amplified Group 3 MB. Therefore, the BTIC-enriched, treatment-refractory MB cells from our PDX model that were specifically collected from mouse spines provide the rare opportunity to investigate this often terminal disease in patients. It is particularly important given the high genetic divergence between recurrent MB and metastatic MB compared to their matched primary tumors, respectively [23, 24].

Here, we performed a high-throughput screen (HTS) of kinase inhibitors to identify candidates against our PDX-generated treatment-refractory, metastatic Group 3 $\gamma$  MB cells. We found that inhibitors that target these BTIC-enriched cells, whilst sparing healthy, human fetal neural stem cells (hNSCs). Our data suggests that further characterization of these inhibitors may provide a new therapeutic strategy for relapsed Group 3 $\gamma$  MB patients with spinal metastasis, who are otherwise often limited to palliative care.

## Materials and methods

### Cell cultures

Treatment-refractory Group 3 MB (SU\_MB002) was obtained from Dr. Yoon-Jae Cho (OR, USA) [23]. Cells were cultured in NeuroCult Complete media (NCC), consisting of NeuroCult™ NS-A Basal Medium (STEMCELL™ technology #05750) supplemented with NeuroCult™ Supplement, 20 ng/mL epidermal growth factor, 10 ng/mL fibroblast growth factor, 0.1% heparin and 1% penicillin–streptomycin. Primary Group 3 MB (HD-MB03) was provided by Dr. Robert Wechsler-Reya (CA, USA) and cultured in NCC with 10% FBS. SHH (DAOY) and Group 4 (ICb-1299) MB cells were cultured in Dulbecco's Modified Eagle Medium (DMEM) with 10% FBS. Cells were plated in NCC 24 h prior to *in vitro* experimentation and intracranial injections. Culture conditions of cells isolated from our PDX model (e.g., HD-MB03-Re-br & sp) remained consistent with original cell lines. HNSCs were isolated and cultured using a previously described protocol [25].

### Inhibitors

HTS compounds were taken from frozen stocks from the David Braley Human Stem Cell Screening Facility; supplied

by the Ontario Institute for Cancer Research (OICR). Top five screen hits were constituted in 10 mM stocks with DMSO.

### High-throughput screening

Z prime ( $Z'$ ) assay and optimization in Supplementary material [26–29]. 2,500 cells/well of HD-MB03-Re-sp were seeded into 96-well tissue culture treated plates by the highly automated, Multidrop™ Combi Reagent Dispenser. The Microlab Nimbus dispensed 1 mM stock of kinase inhibitors into intermediate dilution plates with DMEM and subsequently, resuspended each wells' solution and then transported 20  $\mu$ L/well to corresponding 96-well plates. The screen was conducted in duplicates with 1  $\mu$ M as the final concentration of drugs and controls (0.1% of total well volume). DMSO and puromycin controls were plated at alternating terminals of each row on plates to ensure proper comparison of cell viability with the tested compounds. Following 72-h incubation, PrestoBlue™ was added by the Multidrop™ Combi Reagent Dispenser and fluorescence intensity was measured by the FLUOstar Omega Fluorescence 556 Microplate reader. Cell viability percentage was calculated by dividing the intensity value in the presence of each compound by the DMSO value in the respective row. Mean and standard deviation between duplicates were determined by Omega software. Compounds where one or both replicates indicated 50% or more reduction in cell viability were denoted as screen hits.

### Cell viability assays

2,500 cells/well of single cells of HD-MB03, HD-MB03-Re-br, HD-MB03-Re-sp, SU\_MB002, SU\_MB002-Re-br, SU\_MB002-Re-sp, and hNSCs were sorted by Moflo XDP Cell Sorter into 96-well plates in quadruplicates to determine  $IC_{50}$  values. DMSO was used as the vehicle control. Given the HTS results from testing Group 3 MB cells with compounds at 1  $\mu$ M, cells were treated with four-fold dilutions from 2  $\mu$ M to 7.6 pM (0.1% DMSO or drug). Non-Group 3 MB (DAOY and ICb-1299) cells were treated with two-fold dilutions from 10  $\mu$ M to 9.7 nM. After 72-h incubation, PrestoBlue™ was added. Prism 6 software was used to construct dose response curves and  $IC_{50}$  values by plotting percent cell viability versus transformed dilutions of inhibitors on a logarithmic ( $\log_{10}$ ) scale.  $IC_{80}$  concentrations were calculated with the following formula:  $IC_{(F)} = [(100 - F)/F]^{1/HS} \times IC_{50}$ , where F = desired percent response (i.e., 80 for 80% reduction in cell viability), HS = Hill Slope.

### Sphere formation assays

Limiting dilution assays (LDAs) involved sorting single cells (described above) in quadruplicates at cell densities from 1,000 cells/well to 1 cell/well to compare compounds' self-renewal capacity. Wells with 200 cells/well were used for in vitro secondary sphere formation assays. Following 72-h incubation post-treatment, tumorspheres or colonies (defined as five or more cells in contact with each other) were manually counted. Prism 6 software was used to plot the percentage of wells without spheres at each respective cell density ( $y$ -axis;  $F_0$ ) against the number of cells per well ( $x$ -axis;  $x$ ). To determine the minimal number of cells required to have at least one tumorsphere, the  $y$ -axis must cross the 0.37 level, which was calculated by  $F_0 = e^{-x}$  [30, 31].

### Ex vivo treatment model

All mouse work was in accordance with McMaster University's Animal Research Ethics Board. SU\_MB002 cells were treated with either  $IC_{80}$  of CHIR-124, JNJ-10198409 or DMSO (0.1% total volume) for 72 h in NCC. Following cell collection, Trypan Blue solution (Thermo Fisher Scientific #15250061) was used alongside Countess™ II Automated Cell Counter (Thermo Fisher Scientific #A27977) to ensure that there were equivalent numbers of live cells in each cohort. Cells were then resuspended in 10–12  $\mu$ L of PBS and injected into the frontal lobe of NOD SCID mice ( $n=5$  per cohort) in an unblinded manner using a 10  $\mu$ L Hamilton syringe, as previously described [19].

To assess survival, mice were sacrificed once they reached endpoint. Brains and spines were isolated, formalin-fixed and paraffin-embedded for hematoxylin and eosin (H&E) and human CoxIV staining, respectively. Slide images were taken using the Aperio Slide Scanner and analyzed by ImageScope v11.1.2.760 software (Aperio).

## Results

### High-throughput kinase inhibitor screen for reducing cell viability in Group 3y MB metastatic recurrence cells

We isolated human *MYC*-driven Group 3 MB cells from the spine of relapsed mice (HDMB03-Re-sp) using our established PDX model (Fig. 1a). Preliminary tests involved Z prime ( $Z'$ ) assays (i.e.,  $Z' < 0.5$  indicates a good score with minimal overlap between controls) using



**Fig. 1** High-throughput kinase inhibitor screen targeting metastatic Group 3 $\gamma$  MB cells from recurrence. **a** Schematic representation of PDX therapy model and high-throughput screen. Treatment-naïve Group 3 MB (HD-MB03) cells treated with craniospinal irradiation and subsequently chemotherapy (cisplatin, vincristine and cyclophosphamide) were collected from the spinal cord following recurrence (HD-MB03-Re-sp) and used in this drug screen. **b** Major classes of the compound library used in screen, where the numbers in parentheses specify the number of compounds from each class. **c** Effects on HD-MB03-Re-sp cell viability following compound treatment. Each point is the mean of two technical replicates for a single compound, with percent viability calculated by dividing the cell viability in the presence of the compound by that of DMSO-treated wells for the respective row assayed. The dashed, blue line represents the threshold by which cell viability is reduced by 50%. Error bars represent mean  $\pm$  SD. **d** Stepwise workflow to triage screening hits include BBB permeability via in silico software and reports of toxicity with each tier indicating the number of compounds that met each criterion. **e** Table summarizes the name, structure and targets of five top screen hits. *PI3K* phosphoinositide 3-kinase, *EGFR* epidermal growth factor receptor, *MAPK* mitogen-activated protein kinase, *CDC2* cyclin-dependent kinase, *FLT* fms-like tyrosine kinase, *JAK* janus kinase, *AKT* protein kinase B, *CHK* checkpoint kinase, *KDR* kinase insert domain receptor, *CDK* cyclin-dependent kinase, *PKC* protein kinase C, *PLK* polo-like kinase, *GSK* glycogen synthase kinase, *IGF1R* insulin-like growth factor 1 receptor, *IKK* I kappa B kinase, *PIM* proviral integration site for moloney murine leukemia virus, *TGF $\beta$ R* transforming growth factor beta receptor

puromycin and benlinoestat—a pan-HDAC inhibitor, as positive controls for cell death. To optimize the screen, HD-MB03-Re-sp cells were plated at 500–2,500 cells/well with either 1  $\mu$ M puromycin, benlinoestat or DMSO (0.1% total volume) for 48 or 72 h in one of three media conditions (Supplementary Fig. 1a, b). Based on our previous work and review of the literature, we believed this concentration would not be overly stringent and produce a more suitable number of hits for further investigation. There was no significant difference when comparing media conditions ( $Z' = 0.71, 0.72,$  and  $0.79$  for NCC, DMEM, and NCC + 10% DMEM, respectively for DMSO compared to puromycin); however, the maximal separation between controls was seen in 1  $\mu$ M puromycin versus DMSO at a cell density of 2,500 cells/well, following a 72-h incubation period (Supplementary Fig. 1a, b). We proceeded with screening the 640 kinase library, which includes a wide variety of those tested in preclinical and/or clinical trials, as well as known patented or literature tool compounds that have not yet been rigorously characterized (Fig. 1b). All compounds were evaluated in duplicates at 1  $\mu$ M. As expected, the screening demonstrated a normal distribution with respect to cell viability (Supplementary Fig. 1c). Screen hits were defined as having at least one replicate reducing cell viability by 50% or more. A total of 47 compounds from the 640 screened met this criterion, which is indicated by the blue dashed line (Fig. 1c).

## Distinguishing screen hits based on predicted BBB-permeability

As MB originates in the brain, we reasoned that successful compounds could be administered either alone or in combination with standard chemoradiotherapy to impede or suspend tumor progression and leptomeningeal metastasis. We aimed to further triage the 47 hits based on their blood–brain barrier (BBB) permeability via functional studies. In silico software, Percepta (Supplementary Table 1) and SwissADME (Supplementary Fig. 1d) were used for the analysis. Percepta ([www.acdlabs.com/products/percepta-platform](http://www.acdlabs.com/products/percepta-platform)) measures compounds' toxicity, physiochemical, in addition to absorption, distribution, metabolism, and excretion (ADME) properties. Its BBB (termed CNS) permeability prediction platform takes into account each compound's rate of passive diffusion, as well as distribution ratio of compound in brain tissue and plasma. SwissADME ([www.swissadme.ch](http://www.swissadme.ch)) is a web-based tool that involves the graphical Brain or IntestinaL EstimatedD permeation method (BOILED-Egg), which is based on lipophilicity, established Wildman and Crippen (WlogP) partition coefficient, and topological polar surface area (tPSA) to predict the gastrointestinal absorption and brain penetration of compounds [32, 33]. As predicted by one or both software packages, eight compounds were selected; three of which were eliminated due to prior reports of toxicity (Supplementary Fig. 1e). This workflow is shown in Fig. 1d. The remaining five compounds selected for further evaluation not only targeted aggressive *MYC*-amplified Group 3 MB spinal cells from recurrence, but were also predicted to penetrate the BBB and not reported to be toxic. The targets and respective compounds included Aurora kinase B (AURKB) with Hesperadin, polo like kinase 1 (PLK1) with BI 2536, CHK1 with both CHIR-124 and non-selectively with SB-218078, as well as PDGFR $\beta$  with JNJ-10198409 (Fig. 1e).

## Top screen hits spare hNSCs while inhibiting growth of recurrent metastatic MB BTICs

We validated these findings in an additional biological replicate of Group 3 $\gamma$  MB metastatic recurrence cells (SU\_MB002-Re-sp) and performed dose response studies on hNSCs to determine which compounds did not induce neurotoxicity of healthy neural cells in vitro (Fig. 2). Cell density assays—similar to those from the primary screen, were conducted and again showed 2,500 cells/well densities resulted in the maximal readout values (Supplementary Fig. 2). All compounds except BI 2536 demonstrated varied responses in each Group 3 $\gamma$  MB metastatic recurrence cell lines. Nonetheless, each of the five compounds effectively inhibited cell viability, whilst sparing hNSCs.

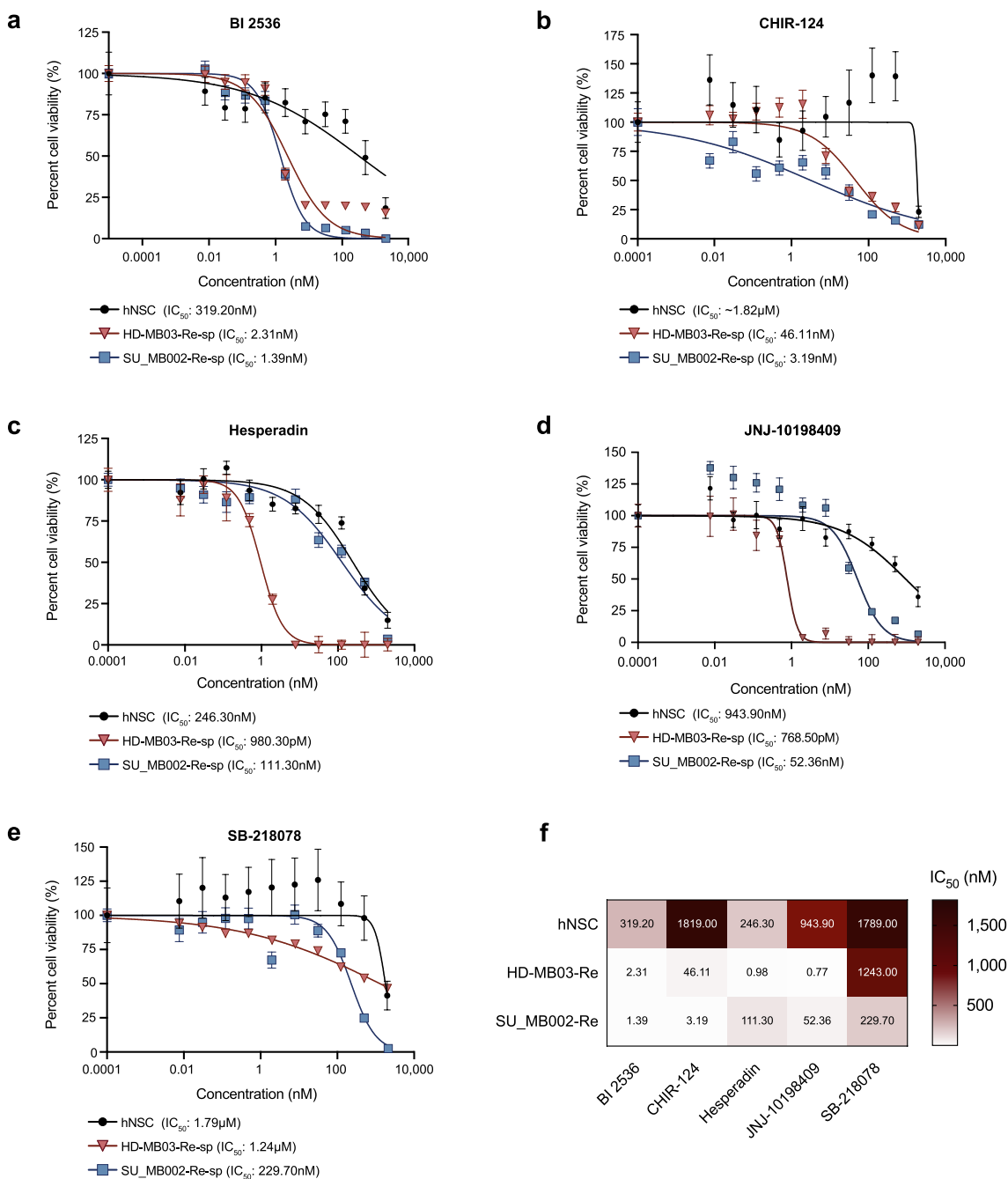


**Fig. 2** Screened kinase inhibitors target metastatic Group 3γ MB cells at tumor recurrence, whilst sparing healthy neural cells. **a** BI 2536, **b** CHIR-124, **c** Hesperadin, **d** JNJ-10198409, and **e** SB-218078 kill metastatic recurrent Group 3γ MB cells (HD-MB03-Re-sp and SU\_MB002-Re-sp) at low nanomolar concentrations, but not neural stem cells (hNSCs) after 72-h treatment. IC<sub>50</sub> values of each compound are

listed beside the respective cell lines. Error bars represent mean ± SD of at least three technical replicates, normalized to DMSO. **f** Summarized heat map of IC<sub>50</sub>s, listed in nanomolar (nM) units, to visually depict the difference in targeting of each compound in the Group 3 MB cells, relative to hNSCs

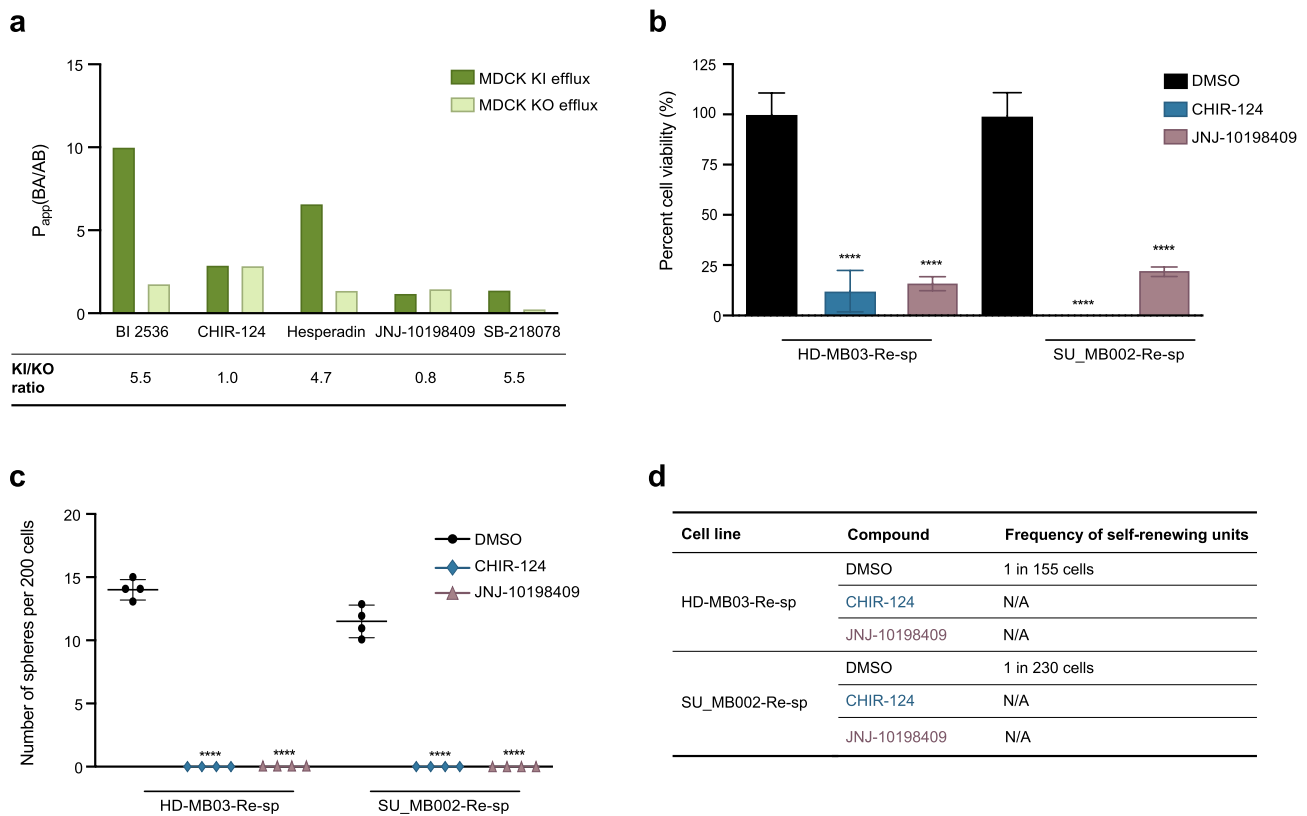


**Fig. 3** Functional in vitro profile of CHK1 (CHIR-124) and PDGFR $\beta$  (JNJ-10198409) inhibitors showing effective BBB permeability and diminished stem cell properties. **a** Results from the MDCKII BBB permeability assay, which demonstrated the KI/KO efflux ratio, where lower values represent less efflux via MDR1 out of the brain. **b** Cell viability, **c** self-renewal capacity, and **d** frequency of self-

renewing units via LDA assays were measured following drug treatment at 0.1% IC<sub>80</sub> concentration or DMSO for 72 h. Error bars represent mean  $\pm$  SD of at least three technical replicates, normalized to DMSO. \* $p \leq 0.05$ , \*\* $p \leq 0.001$ , \*\*\* $p \leq 0.0001$ ; \*\*\*\* $p \leq 0.00001$ ; unpaired *t*-test

To determine which compounds to pursue further, we verified the results from the in silico BBB permeability prediction analysis using an established in vitro BBB permeability assay, termed MDCKII assay. Of note, Percepta predicted that all five compounds except CHIR-124 were BBB penetrable, while SwissADME noted that CHIR-124, JNJ-10198409, and SB-218078 were likely BBB permeable. The MDCKII assay measures BBB permeability and drug efflux. Compounds that undergo active efflux would thereby be transported out of the brain [34]. As hMDR1 is an active efflux transporter, compounds that act as its substrates would indicate poor BBB permeability. For this experiment, hMDR1 KI and cMDR1 KO cells were cultured on polyethylene terephthalate membrane inserts as a monolayer. The cells orient themselves based on polarity into apical and basolateral chambers, representative of blood and brain, respectively (Supplementary Fig. 3). Permeability of compounds from the apical (A) to basolateral (B) chamber and the reverse was tested. The

efflux for each KI and KO cell lines are measured from the permeability ratio of B to A ( $P_{app}$  BA) and A to B ( $P_{app}$  AB) (Supplementary Fig. 3). Those that are not hMDR1 substrates will have a lower KI/KO ratio—indicative of effective brain penetration. We found that CHIR-124 (KI/KO = 1.0) and JNJ-10198409 (KI/KO = 0.8) had low KI/KO ratios, while Hesperadin, BI 2536 and SB-218078 were more similar to the positive control for poor permeability, dinaciclib (Fig. 3a). With this validation, we aimed to further investigate CHIR-124 and JNJ-10198409.

### CHK1 & PDGFR $\beta$ inhibitors significantly impact self-renewal and proliferation of treatment-refractory metastatic MB BTICs in vitro

To assess their role on BTIC properties, functional profiling of these inhibitors upon IC<sub>80</sub> treatment was performed. These studies confirmed that the CHK1 inhibitor CHIR-124 and the dual PDGFR $\beta$  inhibitor JNJ-10198409 target

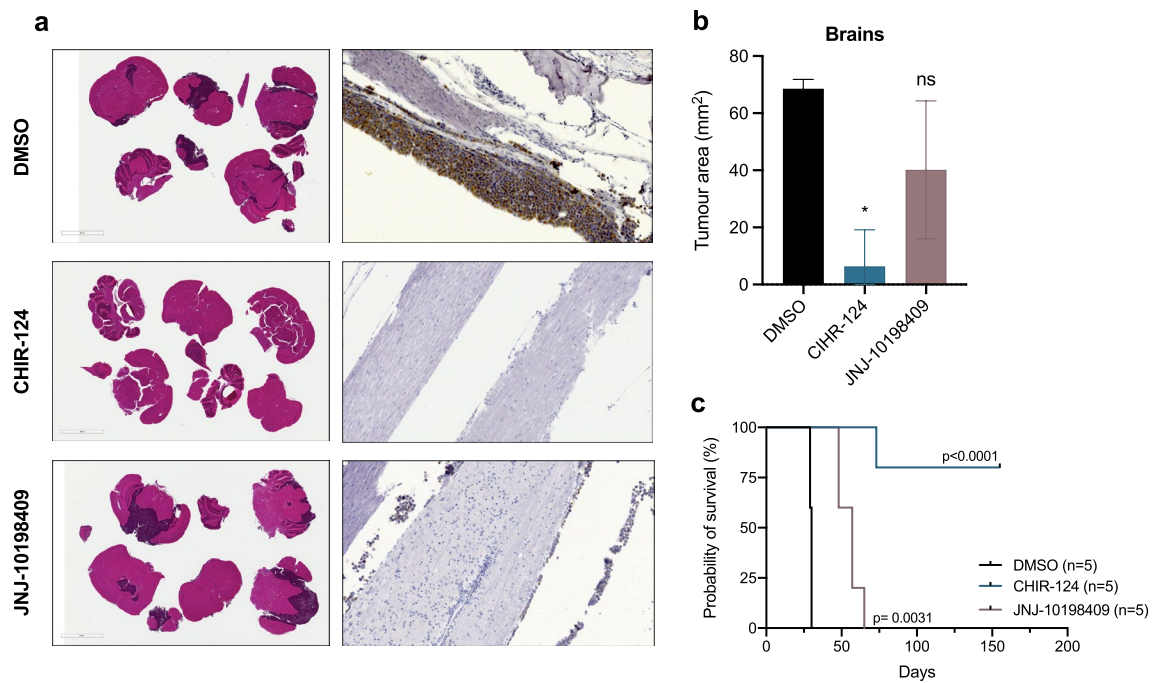


**Fig. 4** Ex vivo effects of CHIR-124 and JNJ-10198409 in *MYC*-Amplified Group 3 MB cells. **a** Representative H&E and immunohistochemistry (IHC) images of mouse brains and spines sections from mouse xenografts of SU\_MB002 cells following either IC<sub>80</sub> drug or DMSO treatment in vitro. Brain and spine sections were stained with hematoxylin and eosin (H&E) and CoxIV, respectively. Spine slides are at 10× magnification. **b** Tumor burden was quantified in brains (n≥3 per cohort), as shown by measuring tumor area. In

spine images only, excess white space between image and scale (mm) was removed to ensure both spine and brain IHC images were similar in size. **c** Prolonged survival benefit was indicated in CHIR-124 ex vivo-treated mice based on the *Kaplan–Meier* curves (n=5 per cohort). Error bars represent mean±SD. \*p≤0.05, \*\*p≤0.001, \*\*\*p≤0.0001; \*\*\*\*p≤0.00001; *unpaired t-test* or one-way ANOVA with Dunnett's method for multiple comparisons

the BTIC sub-population by significantly reducing cell viability and self-renewal capacity of HD-MB03-Re-sp and SU\_MB002-Re-sp through in vitro secondary sphere formation and LDA (Fig. 3c–e). Additional dose response assays were conducted to evaluate whether these inhibitors were also potent in the parental (HD-MB03 and SU\_MB002) and relapsed brain (HD-MB03-Re-br and SU\_MB002-Re-br) cells as a means for potentially, proactive treatment (Supplementary Fig. 4). We also tested non-*MYC*-amplified, non-Group 3 MB cells, DAOY (SHH MB) and ICb-1299 (Group 4 MB) to determine whether the compounds selectively targeted this specific subgroup. Both CHIR-124 and JNJ-10198409 demonstrated nanomolar to low micromolar responses (Supplementary Fig. 5). While the greatest effect was seen in DAOY cells following CHIR-124 treatment, this IC<sub>50</sub> dose was still 2.4× larger than the highest of those in the tested Group 3 MB cells. This may suggest that CHIR-124 and JNJ-10198409 preferentially target *MYC*-driven Group 3 MB lines but further validation is required. Rather, the compounds appear to be more effective whether in parental, relapsed brain or relapsed spine Group 3 MB cells, compared to hNSCs and non-*MYC*-amplified, non-Group 3 MB cells.

### CHK1 inhibitor-treated MB cells formed smaller tumors in vivo & showed increased mouse survival compared to controls

To access the clinical utility of inhibitors, SU\_MB002 cells due to its proven reliability to generate tumors in our previous studies, were treated with the drugs at IC<sub>80</sub> or DMSO after which equal numbers of live cells were injected intracranially into NOD SCID mice. At endpoint, mice were sacrificed to assess tumor burden of brain and spine (Fig. 4a, b), along with survival (Fig. 4c). As expected, quantification of DMSO control mice brains demonstrated increased tumor burden, particularly in comparison to CHIR-124 ex vivo mice. Treated cohorts also exhibited survival benefit, compared to DMSO. Most striking, CHIR-124 ex vivo treatment significantly prolonged survival, whereby 80% of mice remained alive at 155 days post-injection without signs indicative of endpoint; they were sacrificed only to examine brains and spines. Spines from DMSO and JNJ-10198409 cohorts showed human tumor cells as visualized by human CoxIV staining, whereas CHIR-124 spines had complete absence of tumor burden (Fig. 4a).



## Discussion

Current research primarily focuses on MB at diagnosis, despite higher mortality rates in recurrent MB, specifically in *MYC*-amplified Group 3 MB, where tumor recurrence and metastasis are most common. The rare clinical opportunities to collect these samples, the paucity of MB mouse models for metastatic recurrence, and high failure rates of salvage therapies highlight a pivotal gap in current research. Therefore, our work aimed to elucidate effective drug candidates targeting Group 3 $\gamma$  MB metastatic recurrences. While our study does not feature a broad spectrum of agents with varying mechanisms of actions, kinase inhibitors poised a promising drug category to explore given kinases' pertinent role in cell proliferation, migration, differentiation, and apoptosis. Metastatic MB samples even demonstrated upregulation of kinase and growth factor signaling [17]. In conducting a 640-kinase inhibitor HTS, we revealed 47 candidates, which were eventually narrowed down based on *in silico* and *in vitro* BBB-permeability, and reports of toxicity to two top hits—CHK1 (CHIR-124) and PDGFR $\beta$  (JNJ-10198409) inhibitors. This was consistent with high CHK1 expression correlating to poor clinical prognosis in Group 3 $\gamma$  MB and PDGFR $\beta$  overexpression seen in metastatic MB [15, 19, 35].

Both compounds targeted recurrent Group 3 $\gamma$  MB spine cells from our prior PDX model and significantly diminished stem cell properties of these BTIC-enriched cells. This is particularly important given that increased self-renewal capacity in distinct clonal cells at MB diagnosis is postulated to lead to disease progression and dissemination [36, 37]. Also notable was that these compounds did not demonstrate toxicity in healthy hNSCs with a difference in IC<sub>50</sub> values as high as 570-fold for CHIR-124. Moreover, when completing dose response assays in parental and our local recurrence MB PDX cell lines, we anticipated that the IC<sub>50</sub> concentrations of both compounds would demonstrate a uniform, stepwise decrease from parental to relapsed brain or spine cells. However, this was only the case for CHIR-124 in SU\_MB002 when compared to SU\_MB002-Re-br and SU\_MB002-Re-sp; JNJ-10198409 showed a similar trend in HD-MB03 relative to HD-MB03-Re-sp (Supplementary Fig. 4). Although the compounds did exhibit a response in non-*MYC*-amplified, non-Group 3 MB cells, the compounds were more effective at targeting both the original and more aggressive, recurrent cells. This coupled with prior studies of CHK1 inhibition complementing radiotherapy in *MYC*-amplified cells and CHK1 depletion enhancing MB cell sensitivity to cisplatin, suggest that CHIR-124 warrants further investigation with multi-modal therapy in *MYC*-amplified Group 3 MB metastatic recurrences [35, 38, 39]. A recent HTS in commercially-available, primary Group 3 MB cell lines demonstrated synergy between CHK1/2 inhibition and DNA-damaging chemotherapies [40].

In addition, an ongoing clinical trial for recurrent SHH, Group 3 and Group 4 MB patients evaluating another CHK1 inhibitor (LY2606368) in combination with cyclophosphamide or gemcitabine provides validation of our findings [41].

Furthermore, results from our *ex vivo* experiment suggest that CHIR-124 may target the migratory BTIC population prior to injection, leading to such survival benefits. However, additional mouse experiments are warranted to provide further validation. Moreover, an extensive safety profile and pharmacokinetic/pharmacodynamic would allow optimization of dosage and schedule to Group 3 MB, given that both CHIR-124 and JNJ-10198409 are orally bioavailable and well-tolerated in breast and colon cancer PDX models, respectively [42, 43].

Overall, this study provides preclinical insight on two promising inhibitors that target Group 3 $\gamma$  MB metastatic recurrence, which has yet to be fully studied. Future characterization of these inhibitors, especially CHIR-124 in combinatorial therapy, would indicate their clinical utility in treating patients who have limited options available beyond current, ineffective salvage therapies.

**Supplementary Information** The online version contains supplementary material available at <https://doi.org/10.1007/s11060-023-04372-w>.

**Author contributions** AAA, DB, CV and SKS conceived and designed the study. AAA, DB, YK, CV, DU, MS, AA, JM, MKS, DM, CC, NS and MMK-S contributed to the collection of data. AAA, DB, YK, CV, SKS and MMK-S were involved in data analysis and interpretation. AAA wrote the first draft of the manuscript and prepared figures. DB, DU, AA, MS, CV and SKS assisted in further manuscript revisions. All authors read and approved the final manuscript.

**Funding** S.K.S. holds Canada Research Chair award, and operating grants from Canadian Institutes of Health Research (CIHR, #MOP-130317), the Ontario Institute for Cancer Research Cancer Stem Cell Program, Canadian Cancer Society, the Brain Tumor Foundation of Canada, and generous donations from the Box Run Foundation and Team Kelsey Foundation.

**Data availability** The data presented in this study are available in the supplementary material.

## Declarations

**Conflict of interest** The authors have no relevant financial or non-financial interests to disclose.

**Ethical approval** This study was performed in line with the principles of the Declaration of Helsinki. Approval was granted by the Ethics Committee of McMaster University Animal Research Ethics Board (AREB) (April 2019/No.19-01-01).

## References

- Rossi A, Caracciolo V, Russo G, Reiss K, Giordano A (2008) Medulloblastoma: from molecular pathology to therapy. Clin

- Cancer Res 14:971–976. <https://doi.org/10.1158/1078-0432.CCR-07-2072>
2. Mahapatra S, Amsbaugh MJ (2022) Medulloblastoma. In StatPearls. Treasure Island, Florida
  3. Tarbell NJ, Friedman H, Polkinghorne WR, Yock T, Zhou T, Chen Z, Burger P, Barnes P, Kun L (2013) High-risk medulloblastoma: a pediatric oncology group randomized trial of chemotherapy before or after radiation therapy (POG 9031). *J Clin Oncol* 31:2936–2941. <https://doi.org/10.1200/JCO.2012.43.9984>
  4. Ramaswamy V, Remke M, Bouffet E et al (2016) Risk stratification of childhood medulloblastoma in the molecular era: the current consensus. *Acta Neuropathol* 131:821–831. <https://doi.org/10.1007/s00401-016-1569-6>
  5. Northcott PA, Korshunov A, Witt H, Hielscher T, Eberhart CG, Mack S, Bouffet E, Clifford SC, Hawkins CE, French P, Rutka JT, Pfister S, Taylor MD (2011) Medulloblastoma comprises four distinct molecular variants. *J Clin Oncol* 29:1408–1414. <https://doi.org/10.1200/JCO.2009.27.4324>
  6. Taylor MD, Northcott PA, Korshunov A, Remke M, Cho YJ, Clifford SC, Eberhart CG, Parsons DW, Rutkowski S, Gajjar A, Ellison DW, Lichter P, Gilbertson RJ, Pomeroy SL, Kool M, Pfister SM (2012) Molecular subgroups of medulloblastoma: the current consensus. *Acta Neuropathol* 123:465–472. <https://doi.org/10.1007/s00401-011-0922-z>
  7. Northcott PA, Shih DJ, Peacock J et al (2012) Medulloblastoma exome sequencing uncovers subtype-specific somatic mutations. *Nature* 488:106–110. <https://doi.org/10.1038/nature11329>
  8. Taylor RE, Bailey CC, Robinson KJ, Weston CL, Walker DA, Ellison D, Ironside J, Pizer BL, Lashford LS (2005) Outcome for patients with metastatic (M2–3) medulloblastoma treated with SIOP/UKCCSG PNET-3 chemotherapy. *Eur J Cancer (Oxford, England: 1990)* 41:727–734. <https://doi.org/10.1016/j.ejca.2004.12.017>
  9. Wang J, Garancher A, Ramaswamy V, Wechsler-Reya RJ (2018) Medulloblastoma: from molecular subgroups to molecular targeted therapies. *Annu Rev Neurosci* 41:207–232. <https://doi.org/10.1146/annurev-neuro-070815-013838>
  10. Cavalli FMG, Remke M, Rampasek L et al (2017) Intertumoral Heterogeneity within Medulloblastoma Subgroups. *Cancer Cell* 31:737–754.e6. <https://doi.org/10.1016/j.ccell.2017.05.005>
  11. Pei Y, Liu KW, Wang J et al (2016) HDAC and PI3K antagonists cooperate to inhibit growth of MYC-driven medulloblastoma. *Cancer Cell* 29:311–323. <https://doi.org/10.1016/j.ccell.2016.02.011>
  12. Park AK, Lee JY, Cheong H et al (2019) Subgroup-specific prognostic signaling and metabolic pathways in pediatric medulloblastoma. *BMC Cancer* 19:571. <https://doi.org/10.1186/s12885-019-5742-x>
  13. Schoen LF, Craveiro RB, Pietsch T, Moritz T, Troeger A, Jordans S, Dilloo D (2022) The PI3K inhibitor pictilisib and the multikinase inhibitors pazopanib and sorafenib have an impact on Rac1 level and migration of medulloblastoma in vitro. *J Cell Mol Med* 26:5832–5845. <https://doi.org/10.1111/jcmm.17604>
  14. Han Y, Lindner S, Bei Y et al (2019) Synergistic activity of BET inhibitor MK-8628 and PLK inhibitor Volasertib in preclinical models of medulloblastoma. *Cancer Lett* 445:24–33. <https://doi.org/10.1016/j.canlet.2018.12.012>
  15. Gilbertson RJ, Clifford SC (2003) PDGFRB is overexpressed in metastatic medulloblastoma. *Nat Genet* 35:197–198. <https://doi.org/10.1038/ng1103-197>
  16. Abouantoun TJ, Castellino RC, MacDonald TJ (2011) Sunitinib induces PTEN expression and inhibits PDGFR signaling and migration of medulloblastoma cells. *J Neuro-Oncol* 101:215–226. <https://doi.org/10.1007/s11060-010-0259-9>
  17. MacDonald TJ, Brown KM, LaFleur B et al (2001) Expression profiling of medulloblastoma: PDGFRA and the RAS/MAPK pathway as therapeutic targets for metastatic disease. *Nat Genet* 29:143–152. <https://doi.org/10.1038/ng731>
  18. Sabel M, Fleischhack G, Tippelt S et al (2016) Relapse patterns and outcome after relapse in standard risk medulloblastoma: a report from the HIT-SIOP-PNET4 study. *J Neurooncol* 129:515–524. <https://doi.org/10.1007/s11060-016-2202-1>
  19. Bakhshinyan D, Adile AA, Liu J, et al (2021) Temporal profiling of therapy resistance in human medulloblastoma identifies novel targetable drivers of recurrence. *Sci Adv* 7:eabi5568. <https://doi.org/10.1126/sciadv.abi5568>
  20. Singh SK, Clarke ID, Terasaki M, Bonn VE, Hawkins C, Squire J, Dirks PB (2003) Identification of a cancer stem cell in human brain tumors. *Cancer Res* 63:5821–5828
  21. Singh SK, Hawkins C, Clarke ID, Squire JA, Bayani J, Hide T, Henkelman RM, Cusimano MD, Dirks PB (2004) Identification of human brain tumor initiating cells. *Nature* 432:396–401. <https://doi.org/10.1038/nature03128>
  22. Dean M, Fojo T, Bates S (2005) Tumor stem cells and drug resistance. *Nat Rev Cancer* 5:275–284. <https://doi.org/10.1038/nrc1590>
  23. Morrissy AS, Garzia L, Shih DJ et al (2016) Divergent clonal selection dominates medulloblastoma at recurrence. *Nature* 529:351–357. <https://doi.org/10.1038/nature16478>
  24. Wu X, Northcott PA, Dubuc A et al (2012) Clonal selection drives genetic divergence of metastatic medulloblastoma. *Nature* 482:529–533. <https://doi.org/10.1038/nature10825>
  25. Venugopal C, Wang XS, Manoranjan B, McFarlane N, Nolte S, Li M, Murty N, Michael Siu KW, Singh SK (2012) GBM secretome induces transient transformation of human neural precursor cells. *J Neurooncol* 109:457–466. <https://doi.org/10.1007/s11060-012-0917-1>
  26. Dell EJ (2012) The Z prime value (Z'). BMG LABTECH. <https://www.bmglabtech.com/en/blog/the-z-prime-value/>. Accessed 25 Jan 2023
  27. Dukes JD, Whitley P, Chalmers AD (2011) The MDCK variety pack: choosing the right strain. *BMC Cell Biol* 12:43. <https://doi.org/10.1186/1471-2121-12-43>
  28. Volpe DA (2010) Application of method suitability for drug permeability classification. *AAPS J* 12:670–678. <https://doi.org/10.1208/s12248-010-9227-8>
  29. Glauser G, Grund B, Gassner AL, et al (2016) Validation of the Mass-Extraction-Window for Quantitative Methods Using Liquid Chromatography High Resolution Mass Spectrometry. *Anal Chem* 88:3264–3271. <https://doi.org/10.1021/acs.analchem.5b04689>
  30. Bellows CG, Aubin JE (1989) Determination of numbers of osteoprogenitors present in isolated fetal rat calvaria cells in vitro. *Dev Biol* 133:8–13. [https://doi.org/10.1016/0012-1606\(89\)90291-1](https://doi.org/10.1016/0012-1606(89)90291-1)
  31. Tropepe V, Sibilina M, Ciruna BG, Rossant J, Wagner EF, van der Kooy D (1999) Distinct neural stem cells proliferate in response to EGF and FGF in the developing mouse telencephalon. *Dev Biol* 208:166–188. <https://doi.org/10.1006/dbio.1998.9192>
  32. Daina A, Michielin O, Zoete V (2017) SwissADME: a free web tool to evaluate pharmacokinetics, drug-likeness and medicinal chemistry friendliness of small molecules. *Sci Rep* 7:42717. <https://doi.org/10.1038/srep42717>
  33. Daina A, & Zoete V (2016) A BOILED-Egg To Predict Gastrointestinal Absorption and Brain Penetration of Small Molecules. *ChemMedChem* 11: 1117–1121. <https://doi.org/10.1002/cmdc.201600182>
  34. Thiel-Demby VE, Humphreys JE, St John Williams LA, Ellens HM, Shah N, Ayrton AD, Polli JW (2009) Biopharmaceutics classification system: validation and learnings of an in vitro permeability assay. *Mol Pharm* 6:11–18. <https://doi.org/10.1021/mp800122b>
  35. Prince EW, Balakrishnan I, Shah M, et al (2016) Checkpoint kinase 1 expression is an adverse prognostic marker and

- therapeutic target in MYC-driven medulloblastoma. *Oncotarget* 7: 53881–53894. <https://doi.org/10.18632/oncotarget.10692>
36. Reya T, Morrison SJ, Clarke MF, Weissman IL (2001) Stem cells, cancer, and cancer stem cells. *Nature* 414:105–111. <https://doi.org/10.1038/35102167>
37. Wu X, Northcott PA, Dubuc A et al (2012) Clonal selection drives genetic divergence of metastatic medulloblastoma. *Nature* 482:529–533. <https://doi.org/10.1038/nature10825>
38. Wang L, Xiang S, Williams KA, Dong H, Bai W, Nicosia SV, Khochbin S, Bepler G, Zhang X (2012) Depletion of HDAC6 enhances cisplatin-induced DNA damage and apoptosis in non-small cell lung cancer cells. *PLoS One* 7:e44265. <https://doi.org/10.1371/journal.pone.0044265>
39. Wang WJ, Wu SP, Liu JB, Shi YS, Huang X, Zhang QB, Yao KT (2013) MYC regulation of CHK1 and CHK2 promotes radioresistance in a stem cell-like population of nasopharyngeal carcinoma cells. *Cancer Res* 73:1219–1231. <https://doi.org/10.1158/0008-5472.CAN-12-1408>
40. Endersby R, Whitehouse J, Pribnow A, et al (2021) Small-molecule screen reveals synergy of cell cycle checkpoint kinase inhibitors with DNA-damaging chemotherapies in medulloblastoma. *Sci Transl Med* 13: eaba7401. <https://doi.org/10.1126/scitranslmed.aba7401>
41. St. Jude Children's Research Hospital (U.S.) (2019) Evaluation of LY2606368 Therapy in Combination With Cyclophosphamide or Gemcitabine for Children and Adolescents With Refractory or Recurrent Group 3/Group 4 or SHH Medulloblastoma Brain Tumors. Identifier NCT04023669. <https://clinicaltrials.gov/ct2/show/NCT04023669>
42. D'Andrea MR, Mei JM, Tuman RW, Galemno RA, Johnson DL (2005) Validation of in vivo pharmacodynamic activity of a novel PDGF receptor tyrosine kinase inhibitor using immunohistochemistry and quantitative image analysis. *Mol Cancer Ther* 4:1198–1204. <https://doi.org/10.1158/1535-7163.MCT-05-0004>
43. Tse AN, Rendahl KG, Sheikh T, Cheema H, Aardalen K, Embry M, Ma S, Moler EJ, Ni ZJ, Lopes de Menezes DE, Hibner B, Gesner TG, Schwartz GK (2007) CHIR-124, a novel potent inhibitor of Chk1, potentiates the cytotoxicity of topoisomerase I poisons in vitro and in vivo. *Clin Cancer Res* 13:591–602. <https://doi.org/10.1158/1078-0432.CCR-06-1424>

**Publisher's Note** Springer Nature remains neutral with regard to jurisdictional claims in published maps and institutional affiliations.

Springer Nature or its licensor (e.g. a society or other partner) holds exclusive rights to this article under a publishing agreement with the author(s) or other rightsholder(s); author self-archiving of the accepted manuscript version of this article is solely governed by the terms of such publishing agreement and applicable law.